Archives of Biochemistry and Biophysics 605 (2016) 41–48

Contents lists available at ScienceDirect

Archives of Biochemistry and Biophysics

journal homepage: www.elsevier.com/locate/yabbi

Low temperature plasma processing for cell growth inspired carbon thin films fabrication

Manish Kumar [a, *], Jin Xiang Piao [a], Su Bong Jin [a], Jung Heon Lee [b], Satomi Tajima [c], Masaru Hori [c], Jeon Geon Han [a, **]

[a] Center for Advanced Plasma Surface Technology, NU-SKKU Joint Institute for Plasma-Nano Materials, School of Advanced Materials Science and Engineering, Sungkyunkwan University, Suwon, 440-746, South Korea
[b] Biological & Nanoscale Materials Lab, Advanced Materials Science and Engineering, Sungkyunkwan University, Suwon, 440-746, South Korea
[c] Plasma Nanotechnology Research Center, Nagoya University, Furo-cho, Chikusa-ku, 4648603, Japan

ARTICLE INFO

Article history:
Received 31 December 2015
Received in revised form
22 March 2016
Accepted 25 March 2016
Available online 30 March 2016

Keywords:
Carbon
Cell cultivation
Photoelectron spectroscopy
Low temperature plasma
Bone cell

ABSTRACT

The recent bio-applications (*i.e.* bio-sensing, tissue engineering and cell proliferation etc.) are driving the fundamental research in carbon based materials with functional perspectives. High stability in carbon based coatings usually demands the high density deposition. However, the standard techniques, used for the large area and high throughput deposition of crystalline carbon films, often require very high temperature processing (typically >800 °C in inert atmosphere). Here, we present a low temperature (<150 °C) pulsed-DC plasma sputtering process, which enables sufficient ion flux to deposit dense unhydrogenated carbon thin films without any need of substrate-bias or post-deposition thermal treatments. It is found that the control over plasma power density and pulsed frequency governs the density and kinetic energy of carbon ions participating during the film growth. Subsequently, it controls the contents of sp^3 and sp^2 hybridizations via conversion of sp^2 to sp^3 hybridization by ion's energy relaxation. The role of plasma parameters on the chemical and surface properties are presented and correlated to the bio-activity. Bioactivity tests, carried out in mouse fibroblast L-929 and Sarcoma osteogenic (Saos-2) bone cell lines, demonstrate promising cell-proliferation in these films.

1. Introduction

Carbon thin films offer a wide range of exceptional physical, mechanical, biomedical and tribological properties that makes them scientifically fascinating and commercially essential for numerous industrial applications. Conventionally, carbon films have two structural extremes; the hard diamond-like phase with sp^3 bonds and the softer graphite-like phase with sp^2 bonds. The phases with majority of sp^3 bonds percentages; the diamond (100%), nc-diamond (>90%), and diamond-like carbon (80–90%) are preferred as protective coatings, as micro-electromechanical devices, as nanomechanical-based sensors and actuators [1–3]. Whereas, the films with majority of sp^2 bonds are found suitable for electrochemical, supercapacitors, sensors or fuel cells applications [4–6]. It has been reported that carbon electrodes can possess a high loading of electrochemically active dopants for excellent supercapacitors performance [4]. As an organic electrode, its superiority to Pt based electrodes has been shown for next generation neural interfaces [5]. Owing to the tailored microstructures and surface area, carbon films were also applied in photovoltaics [7], gas separation [8] and bio-applications [9–12]. Particularly for bio-applications, the interesting electrochemical properties of carbon have found large potential window for water splitting reactions, enhancing its selectivity for bio-molecule sensing. Apart this, introduction of chemical functionalities has also been reported for cell-proliferation [12]. Conventionally diamond-like carbon was used for cell-cultivation applications [10,11]. But higher processing temperature for diamond-like carbon restricts its use on flexible substrate. This demands the need of identifying other forms of carbon or the processing advances which can be suitable for the cell-growth inspired carbon films. Nanocrystalline carbon (nc-C), which has coexisting threefold (sp^2 bonding) and fourfold (sp^3) bonding coordination, can be an interesting choice in this direction. Though the sp^3 and sp^2 bonds have short range order only, the

* Corresponding author.
** Corresponding author.
E-mail addresses: manishk@skku.edu (M. Kumar), hanjg@skku.edu (J.G. Han).

http://dx.doi.org/10.1016/j.abb.2016.03.026
0003-9861/

bonds casually can intermix and exhibit extended order on nano-scale [13]. By adjusting the ratio of sp^2 to sp^3 bonds in the deposited films, one can obtain the desired functional properties of the films. However, the correlation of carbon hybridizations is sparsely studied in relation to bio-applications.

Varieties of synthesis techniques i.e. photocatalytic process [14], chemical vapour deposition [8,15], magnetron sputtering [12,16–18] etc. are reported for the deposition of carbon films. Considering the industrial needs (i.e. purity, fast process, environmental safety and simple processing steps), sputtering based techniques are preferred over others. Using RF sputtering process (having ion energies in the range of 50–120 eV) nucleation of nc-graphite/diamond clusters is reported to be initiated at temperature in the range of 23–93 °C [16]. However, most of the DC-sputtering induced films usually remain amorphous unless processing is not supplemented with additional physical energy (substrate temperature, post deposition annealing, substrate bias etc.). Evolution of nc-C by aggregation of sp^2 clusters was suggested in the presence of relatively high pressures [1], but recent report, on the effect of working pressure enhancement, showed the porosity enhancement in the films [19]. From, post deposition annealing point of view, crystallization of amorphous-C, in inert atmosphere, usually starts at temperature higher than 800 °C. Annealing in atmospheric conditions had shown the transition temperature as low as 200 °C, where catalytic effect of oxygen initiated the nucleation process [20]. It should be mentioned here that catalytic action turns the film structure as porous, hence it should be avoided if the objective is to find a stable dense coating. Considering these reports and the underlying limitations, we hypothesized that enhancing the ionization of neutral species and kinetic energy of ions/neutrals during the sputtering process can be suitable for preparation of nc-C films. For investigating our hypothesis, we employed addition of pulse frequencies on high power density.

We present here the methodology to deposit good quality unhydrogenated nc-C thin films at low temperatures (without the requirements of any substrate temperature or biasing). The roles of power density and pulse frequency on the film growth, surface energy and chemical bonding of deposited thin films have been presented in details. Finally, the cell viability of mouse fibroblast L-929 and Saos-2 bone cells on the deposited films has been demonstrated.

2. Experimental details

2.1. Film preparation

The films were deposited in a rectangular parallelepiped vacuum chamber, schematically shown in Fig. 1. The chamber consists of an unbalanced magnetron sputtering source, electromagnets and connected power coils to create the magnetic field. The sputtering target was 99.999% pure graphite (circular shaped with 4 inch diameter), fitted with water cooled copper backing plate. In front of the sputtering target, substrates were mounted at the distance of 6 cm on the substrate holder in vertical position. The substrate holder was attached to a rotating platform (20 cm diameter), which was rotated clockwise with rotational speed 20 rpm. The chamber was evacuated using a turbo molecular pump assisted with a rotary pump. The base pressure was maintained below 3×10^{-2} mTorr and the working pressure was fixed at 3 mTorr by maintaining the appropriate Ar gas flow. DC power was applied on the graphite target to maintain the power density variations as 10, 15, 20, 25 and 30 W/cm^2. Further, at constant 25 W/cm^2 power density and 2.9 μs duty time, pulsed frequencies were varied as 50 kHz, 100 kHz, and 150 kHz. The borosilicate glass and Si wafer were used as substrates. Before deposition, substrates were cleaned with acetone and ethanol for 15 min sequentially using ultrasonic cleaning, followed by drying using air gun.

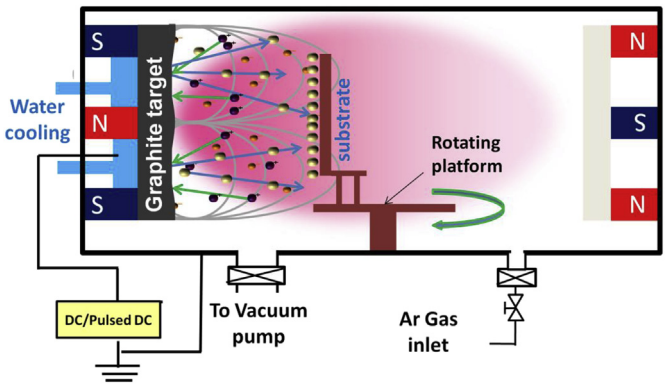

Fig. 1. Schematic diagram of the unbalanced pulsed DC-magnetron chamber for low temperature plasma processing for carbon thin films. Closed-loop lines, dark red, dark green and smaller light brown spheres represent the magnetic field lines, Ar ions, C ions/neutrals and electrons, respectively (not in scale).

2.2. Characterization techniques

The thickness of the deposited films was measured using α-step profiler (KLA Tencor Alpha-step IQ). Substrate temperature was monitored using a temperature monitor (HANYOUNG NUX, DX3) which employs K-type sensor. Field emission scanning electron microscopy FESEM (JEOL JSM-6500F) was employed to investigate the surface morphology of the films by imaging secondary electrons at fixed working distance 7.9 mm and primary electron beam of energy 10 keV. Chemical properties of the films were studied using X-ray photoelectron spectroscopy (XPS) using MultiLab 2000 spectrometer (Thermo Electron Corporation, UK) with monochromatic Al source. Chemical information of the films is studied using high resolution core level study. The XPS spectra were recorded without the surface etching, however samples were preserved to atmospheric exposure by keeping inside vacuum boxes between the duration of sample preparation and XPS characterizations. Raman spectroscopy was carried using 532 nm source wavelength (Alpha 300 M, WI Tec). Contact angle measurements were carried out using sessile drop method. A drop of distilled water (of 4 μL volume) was carefully dropped on to the film-surface, followed by capturing the drop profile using the adjacent camera. Measurements were recorded at different places and contact angle was calculated as average of five measurements. The same procedure was repeated with di-iodo-methane (in place of distilled water) to measure the contact angle with nonpolar component.

2.3. Cell viability

The films were deposited on round borosilicate glass substrate (of 15 mm diameter) for *in-vitro* cell-cultivation study using L-929 (at Sungkyunkwan University, Korea) and Saos-2 (in Nagoya University, Japan) cell lines. For the L-929 cell line, the culture medium contained 89% RPMI-1640 (Nutritious solution), 1% antibiotics (penicillin and streptomycin) and 10% fetal bovine serum (FBS- RM Bio USA). The cells containing medium was incubated for 24 h at 37 °C in 5% CO_2 for normalization. The sterilization of deposited films was performed by UV treatment for 15 min and then the films were put into 24 well plates. One day after first cell seeding corresponded to 0 h, and then viability was measured after 24 h and 120 h using the MTT assay method. For each measurement, the

medium in each well was exchanged with MTT (3-(4,5-dimethylthiazol-2-yl)-2,5-diphenyltetrazolium bromide, Calbiochem, Germany) and incubated for 3 h. Then the medium was exchanged with DMSO (dimethyl sulfoxide) and optical absorption was measured at fixed wavelength 570 nm.

Serum free DMEM medium (Dulbecco's modified Eagle's medium) procured from (Nissui Pharmaceutical Co. Tokyo, Japan) and supplemented with 10% FBS (fetal bovine serum) and 1% PS (penicillin and streptomycin) was used to incubate the Saos-2 cells. The culture medium was normalized at 37 °C in 5% CO_2 for 24 h. The films were put into 24 well plates for cell seeding. Each well contained 600 μL medium. The first day of normalization after seeding cells, corresponded to 0 h, and cell-viability was checked after 24 h and 48 h using the cell counting kit (CCK-8) assay method. The 40 μL of CCK-8 was put in each well and after 4 h, 400 μL medium was extracted from the well to measure the optical absorption.

3. Results and discussion

The thicknesses of the films were kept constant as 200 nm (±5%) by varying the deposition time; depending on the growth rate obtained in each experimental condition. The effects of plasma conditions on growth rate and substrate temperature are presented in Fig. 2. The variation in growth rate of the films is shown in Fig. 2(a) as a function of power density and pulse frequency. Here, it is evident that power density controls the growth rate prominently and has almost a linear dependence. Whereas, the pulse frequency variation doesn't show any systematic variation in deposition rate. Considering the accuracy of thickness measurement, the variation in growth rate may be regarded almost constant as a function of pulse frequency. Here, it should be noted that at power density 30 W/cm^2 and at frequency 150 kHz, plasma was having slight instability. Thus, for safe and reliable plasma processing, the higher limits of power density and pulse frequency were kept as 25 W/cm^2 and 100 kHz, respectively.

Substrate temperature is an important plasma characteristics governed by the impact of neutrals and ions onto the substrate. It depicts the energy consumption in thermal relaxation mode during the film deposition. In static substrate platform mode, the effect of variation in power density (at fixed frequency of 100 kHz) and variation in pulse frequency (at fixed power density 25 W/cm^2) on the substrate temperature are shown in plots of Fig. 2(b)–(c), respectively. Substrate temperature is monitored for 30 min (sufficiently more than actual deposition time used in this works). It is observed that substrate temperature instantaneously rises (well below than 1 min) and then saturates for all conditions of power density variation. Further, the rate of reaching to maximum temperature was found to be higher for higher power density. The maximum substrate temperature was recorded around 465 °C for the power density 25 W/cm^2. When, pulse frequency was varied from 50 kHz to 150 kHz (at fixed power density 25 W/cm^2), substrate temperature was found to be increased from 325 °C to 748 °C.

With the objective of lowering the substrate temperature, the substrate holder platform was rotated with 20 rpm. Since it is not possible to monitor the substrate temperature in rotating condition, we modeled the equivalent experiment using the tapping supply of pulsed power (for the fixed plasma power condition; power 25 W/cm^2 and pulse frequency 150 kHz). As shown in Fig. 2(d), the on-time of plasma pulse was maintained as 0.18 s (±0.04 s), and off-time as 2.82 s. Since rotation speed is 20 rpm, the platform takes 3 s in one rotation. Considering the 62.83 cm circumference of the platform, the used on-time plasma pulse (=

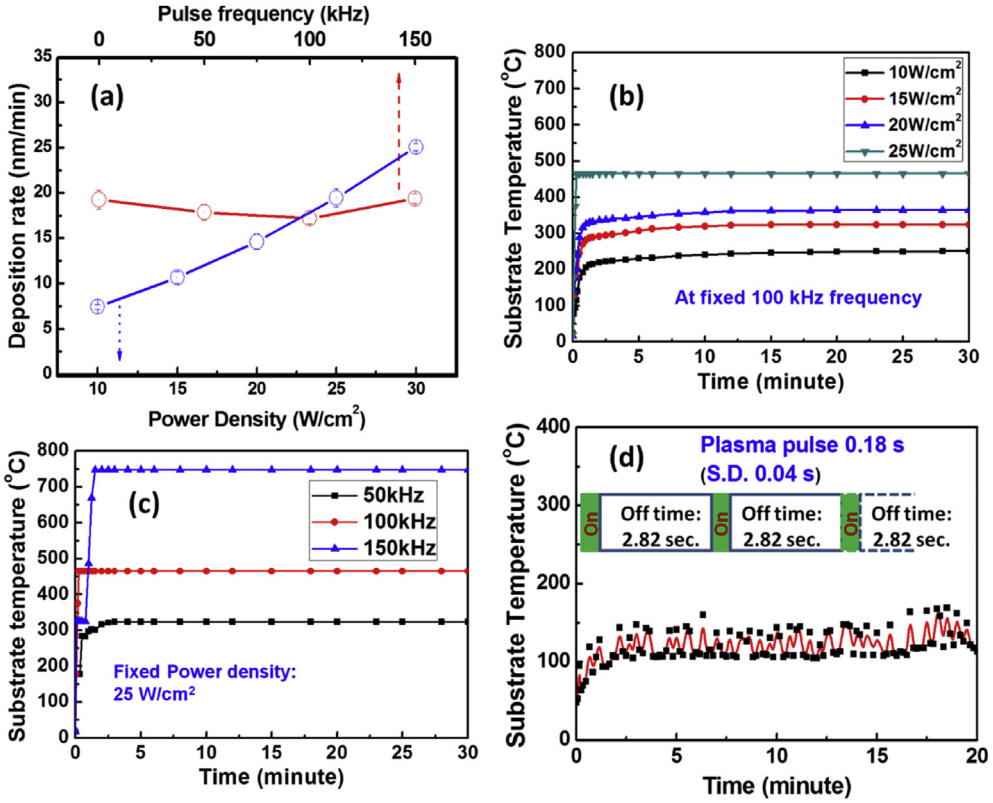

Fig. 2. Plasma diagnostic during the synthesis: (a) The variation of film growth rate as a function of power density and pulsed frequencies. The effect of variation in (b) power density and (c) pulsed frequencies during the plasma process on the plasma induced substrate-temperature (in static mode condition of substrate holder platform). (d) Substrate temperature variation in rotating mode condition of substrate holder platform (for fixed plasma power conditions of 25 W/cm^2 power density and 150 kHz frequency).

0.18 s) allows the plasma interaction-width at the substrate location as 3.77 cm. This width is assumed appropriate for the substrate (of 1 cm width) exposed prominently to the plasma in one rotation. Under this assumption, the substrate temperature was recorded for 20 min at the interval of 5 s, as shown as the plot in Fig. 2(d). Here, it is clearly evident that using such rotating mode of the substrate holder platform provides drastic decrease in the substrate temperature from 748 °C (in static mode) to less than 150 °C, under same power density and pulse frequency. Hence, the combination of pulsed power operation (for higher ionization during plasma process), and tapping pulse (for modeling the plasma-substrate interaction time) in rotating substrate condition provides the advantage of uniform deposition on multiple samples (mountable across the periphery of sample holder platform) as well as controlled substrate temperature.

Surface morphology of the deposited films was studied using FESEM images recorded at 100000× magnifications, as shown in Fig. 3. Here, micrographs (a), (b), (c), and (d) are corresponding to the films prepared by 10, 15, 20 and 25 W/cm^2 power density. Whereas, micrographs (e) and (f) are corresponding to films prepared using 50 kHz and 100 kHz pulse frequency at fixed 25 W/cm^2 power density. The images of the films in top-view show that all films are uniformly and densely deposited. The surface morphology also reveals the nucleation in the form of nanocrystals (<5 nm size), and aggregation of nanocrystals in the form of nanodomains, as clearly shown in the inset of micrograph (a). The dimensions of these nanodomains are found to slightly decrease with enhancing the power density and with the pulse frequency. The decrease in the size of nanodomain is an indication of enhancing the density of the film. In a previous work, we have shown that sputtering induced carbon nanodomains are responsible for the surface conductivity and also correspond to bulk conductivity of the films [17].

The C-*1s* core level spectra of the films are shown in Fig. 4, where (a), (b), (c), (d), (e), and (f) spectra correspond to the films deposited at power densities 10, 15, 20, 25, 25 (with pulse frequency 50 kHz) and 25 (with pulse frequency 100 kHz) W/cm^2, respectively. For identification of different components of C-hybridizations, quantitative analysis was carried out using the *XPSPEAK 4.1* software. Tougaard baseline fitting was done in all spectra. For the Tougaard background, this program optimises the *B1* parameter by minimising the "square of the difference" of the intensities of ten data points in the high binding energy side of the range with the intensities of the calculated background. After fixing the range of binding energy as 280–290 eV, and averaging 5 points at end-points, *B1* parameter was optimized as 22894.94, 21758.75, 25559.35, 23390.48, 25213.88 and 28525.68, for the films deposited at power densities 10, 15, 20, 25, 25 (with pulse frequency 50 kHz) and 25 (with pulse frequency 100 kHz) W/cm^2, respectively. The asymmetric broad peak of C-*1s* is deconvoluted into three components. The components at binding energies 284.2 eV (±0.1 eV), 285.2 eV (±0.1 eV) and at 288.2 eV (±0.1 eV) are assigned to be due to sp^2, sp^3 and C bonded with O. Such assignment is adopted from the literature [21,22]. All core level spectra look very much similar in visual appearance. Thus, for the deeper insight, quantification of sp^2, sp^3 and C bonded with O component was done on the basis of area under these component peaks. The contributions of these three components as a function of (a) power density and (b) frequency are shown in Fig. 5. It is clear from these plots that contribution from C bonded to O is very low (in the range of 4.3%–4.9%). The maximum of this (4.9%) occurs in the film deposited at lowest power density (10 W/cm^2). We anticipate that in sputtering induced carbon films, the top layer usually grows due to low energy species. This condition normally yields amorphous carbon at the top layer, and this layer is more prone to the affected by the atmospheric oxygen. Fig. 5(a) exhibits that enhancing the power density increases the contribution of sp^2 hybridization and decreases the contribution of sp^3. Whereas the role of pulse frequency, as shown in Fig. 5(b), is found to be just reverse. It should be noted that through the relative contributions of sp^3 and sp^2, more information about the π bonds (governing the electronic properties) and σ bonds (governing the mechanical properties) can be found [21]. Overall, the present XPS results demonstrated the correlation of plasma parameters for controlling the sp^3 and sp^2 content in unhydrogenated carbon films.

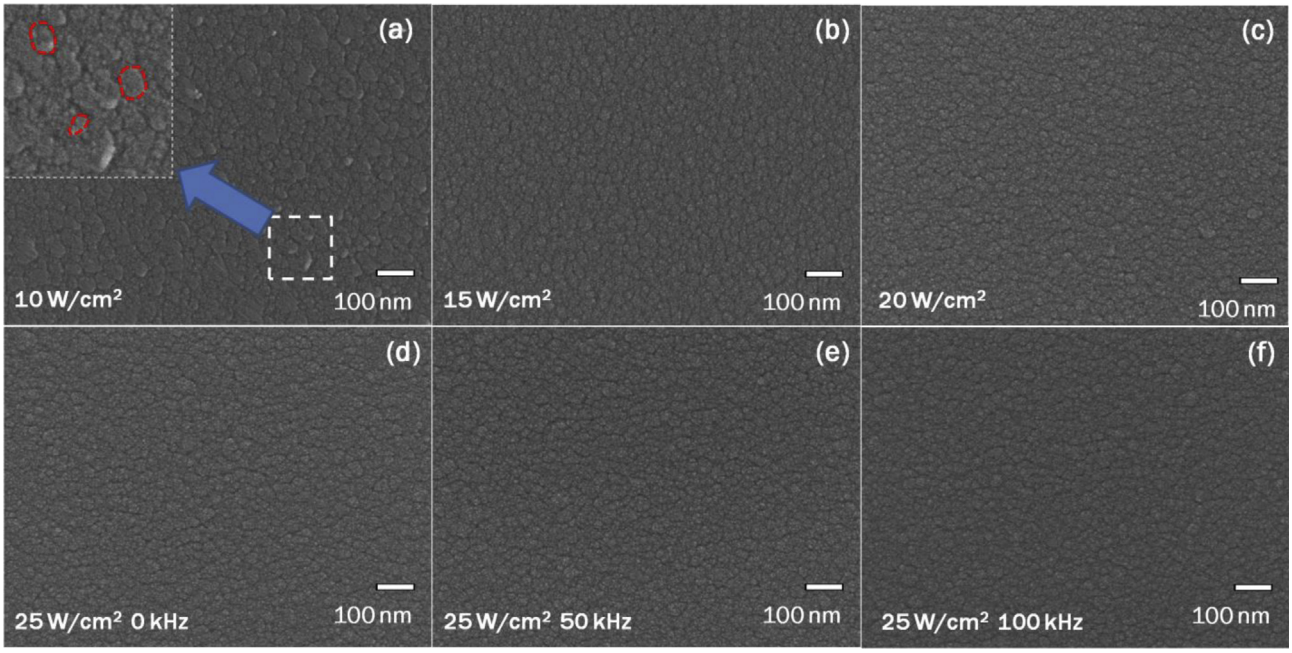

Fig. 3. Effect of plasma power conditions on surface morphology: FESEM images of the films deposited using power densities (a) 10 W/cm^2, (b) 15 W/cm^2, (c) 20 W/cm^2, (d) 25 W/cm^2, (e) 25 W/cm^2 with pulse frequency 50 kHz and (f) 25 W/cm^2 with pulse frequency 100 kHz.

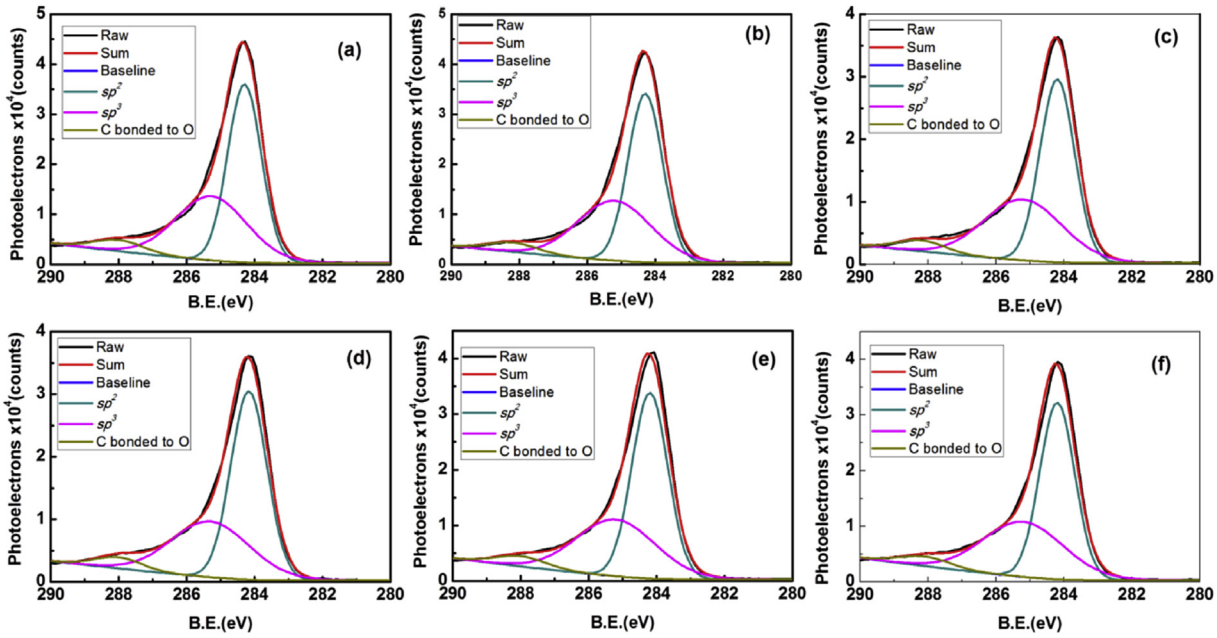

Fig. 4. Effect of plasma power conditions on chemical bonding states: (a) Core level spectra of C-*1s* of films deposited using power densities (a) 10 W/cm^2, (b) 15 W/cm^2, (c) 20 W/cm^2, (d) 25 W/cm^2, (e) 25 W/cm^2 with pulse frequency 50 kHz and (f) 25 W/cm^2 with pulse frequency 100 kHz.

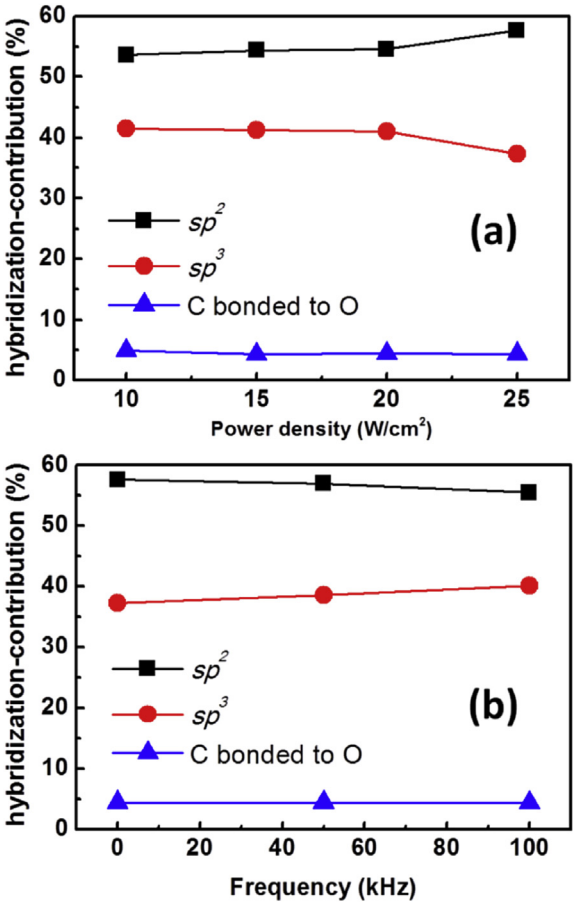

Fig. 5. The contributions of sp^2 and sp^3 hybridization with varying the (a) plasma power density and (b) frequency.

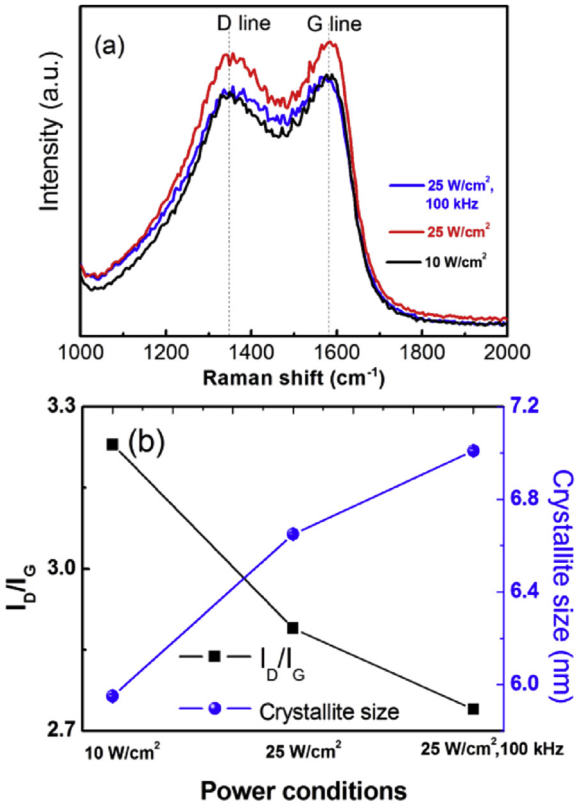

Fig. 6. Raman spectroscopy of films prepared in plasma power conditions (10 W/cm^2, 25 W/cm^2, and 25 W/cm^2 with 100 kHz pulse frequency): (a) Raw Raman spectra (b) corresponding I_D/I_G ratio and crystallite size.

Further confirmation about the microstructure and crystallinity information was obtained by Raman spectroscopy of films prepared in extreme plasma power conditions (pure DC minimum power, maximum power, and pulsed DC maximum power). Fig. 6(a) shows

the raw data of intensities as a function of Raman shift in the range of 1000–2000 cm^{-1}. Here all films show distinct G bands (due to crystallite of graphite) along with the D band (due to the disorder in graphite). For quantitative information, each spectrum was deconvoluted into two Gaussian peaks and ratio of I_D/I_G was calculated on the basis of area under peaks. Using the values of I_D/I_G and the wavelength of laser, the crystallite size of graphite was calculated using the expression given by Cançado et al. [23]. The variation in I_D/I_G ratio and crystallite size is shown in Fig. 6(b). From the plots, it is clear that higher power and frequency conditions induce slight increase in the crystallite size from 5.95 nm to 7.01 nm.

Surface energy of the carbon films is studied using the contact angles of polar and nonpolar liquids. Surface energy is calculated using the Fowkes model, which combines the Young and Young-Dupree equations and considers the dissociation of liquid and solid surface energy into its polar and nonpolar components [24,25]. The effect of (a) power density and (b) pulse frequency on the contact angle of water and diiodomethane, and on the surface energy of the films is shown in Fig. 7. It is evident that in all conditions, films remain hydrophilic and their contact angles do not vary much with the power density, however a small increase in the contact angle is seen with the increase of frequency. The surface energy values were found to slightly increase from 53.59 mJ/m^2 to 54.43 mJ/m^2 on increasing the power density, where as decreasing from 54.43 mJ/m^2 to 52.69 54.43 mJ/m^2 on increasing the pulse frequency. With these results, it is clear that pulse frequency (in comparison to plasma power) plays dominant role in governing the surface energy.

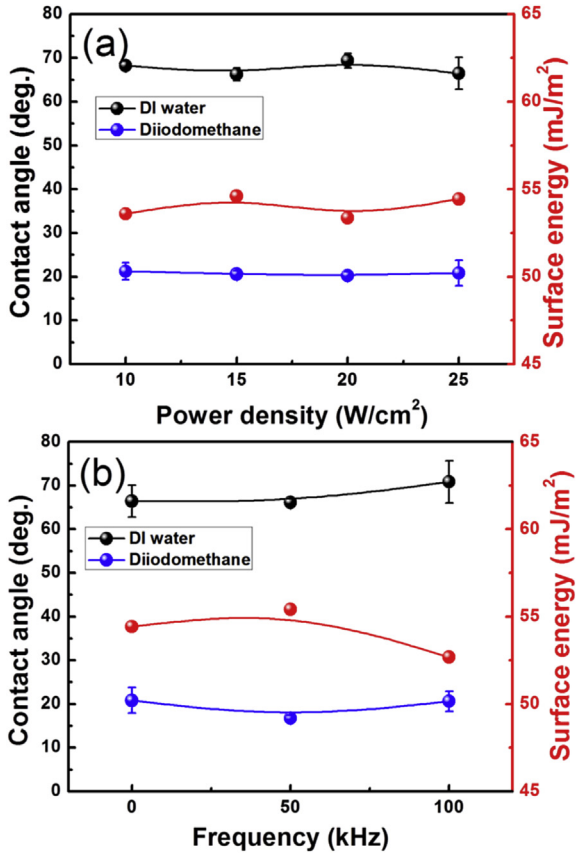

Fig. 7. Wetting properties and surface energy study: The variation in (a) water contact angles and (b) surface energy of the thin films as a function of power density and pulse frequencies.

The growth of L-929 mouse fibroblast, and Saos-2 bone cells was investigated on the deposited carbon films under varying power density and frequency. The growth rate of the cells was estimated using a linear correlation of cell counts to optical absorbance. The viability is normalized with respect to the well-plate with culture without carbon films (as 100%) under identical experimental conditions (after 24 h of culture normalization). Normalized viability of L-929 cells on the carbon films, deposited at different power density and frequency, is shown as histograms (a) and (b), respectively in Fig. 8. Similarly, normalized viability of Saos-2 cells on the carbon films, deposited at different power density and frequency, is shown as histograms (c) and (d), respectively in Fig. 8. From the histograms, it is clear that present carbon films have good cell-adhesivity and affinity for both kind of cells cultivation. The growth rate for Saos-2 cells was higher in comparison of L-929 cells. With the variation of power density, any systematic variation is not observed in either of L-929 or Saos-2 cell viability. However, with the results of viability with frequency variation, it can be deduced that films deposited at lower frequencies (pure DC) are suitable for L-929 cell-cultivation where as films deposited at higher frequencies are suitable for Saos-2 cell cultivation. The higher affinity of Saos-2 cells towards films of higher surface energy (prepared at high pulse frequency) is in agreement to the linear correlation reported earlier for cell-material interaction [24]. Whereas, L-929 cells do not behave in similar way corresponding to surface energy variation. For such behaviour, we recall that increase in pulse frequency decreases the sp^2 content, as shown in Fig. 5. Since, conductive carbon films are reported as favourable for L-929 cell growth [18], the slight decrease in overall sp^2 content can be responsible for the relative decrease in viability of L-929 cells.

The bio-activity of various forms of C materials (specific to Saos-2 and L-929 cells) are compared in Table 1. It is found that single walled carbon nanotubes [27], nc-Diamond [27,28], carbon nanowalls layers [30] and pyrolysis derived micro-patterned carbon [31] generally have a negative affinity for the cell-growth. Patterned diamond films have shown cell-affinity of Saos-2 towards the O-terminated patterns (having higher wettability) in comparison to H-terminated patterns (having lower wettability) [29]. Carbon-carbon composites [32] and carbon nanofibers [33] have shown almost no growth of L-929. So far, only diamond like carbons [26,34] and conductive carbon films [18] have shown cell growth. However, the quantitative comparison of cell-growth exhibits the superiority of present films on others for cell-viability of Saos-2 and L-929 cells.

In present work, good quality (from stability point of view) and uniform growth of the dense carbon films was established by the FESEM results. It is important to be noted that at fixed power density 25 W/cm^2 and 150 kHz frequency condition, the substrate temperature is reduced from the 748 °C to below 150 °C. Since, films were prepared with even less frequencies (100 kHz), it is expected that the actual substrate is even far lower than 150 °C. Apart the lowering substrate temperature, the use of rotating platform allows coating on cylindrical shapes and simultaneous coatings on multiple samples owing to the available total circumference of 62.83 cm. As shown in XPS results, the power density increases sp^2 content, whereas frequency addition increases the sp^3 content. Considering that pulse frequency addition doesn't change deposition rate significantly, it can be stated that the role of pulse frequency in present case is to provide more energy to the ions/neutral species during the sputtering process. Such additional energy is used for the conversion of sp^2 to sp^3 hybridizations, as observed in XPS results. The ion flux (not shown here) was found to be increased with the frequency, which suggests that ionization of neutrals increases with the enhancement of frequency. Thus deposition rate remains same. The role of power density can be

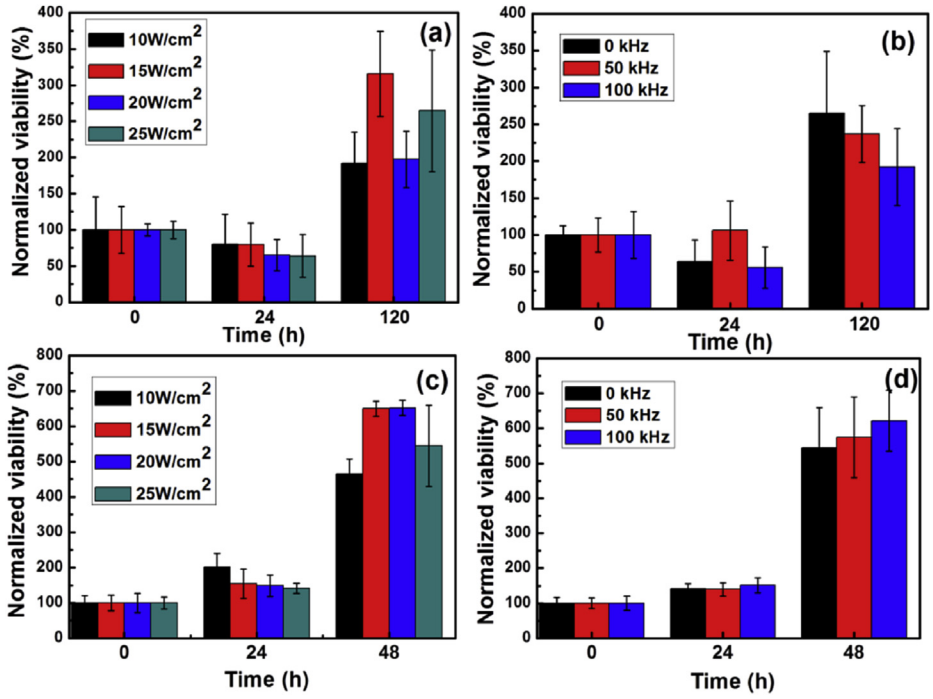

Fig. 8. Effect of plasma power conditions on cell-cultivation on films: Normalized viability as a function of time for the L-929 mouse cells with varying (a) power density and (b) pulse frequency. Normalized viability as a function of time for the Saos-2 bone cells with varying (c) power density and (d) pulse frequency.

Table 1
Comparison of bio-activity towards Saos-2 and L-929 cells in different forms of carbon materials.

Type of cells	Synthesis technique	Type of carbon	Bio-activity	% cell growth	Incubation period	Findings/ Comments
Saos-2	Fast atom bombardment, Plasma assisted CVD	Diamond like carbon [26]	Proliferation	~100%	1 day-3 days	• no. of cells increases with the incubation period
	Laser ablation, arc-discharge, and hiPco	Single walled carbon nanotubes [27]	Metabolic activity	Negative		• metabolic activity decreases ~15 % in comparison to control • no effect of synthesis technique/ impurities
	Microwave plasma CVD	nc-diamond [27]		Negative		• metabolic activity decreases ~15 % in comparison to control • decrease independent of surface roughness
		nc-diamond/a-C nanocomposite films [28]	Cytotoxicity	Slightly negative		• Not cytotoxic, but number of cells are slightly lower than control
		Patterned diamond films [29]	Adhesivity			•Cells strongly prefer O terminated patterns (having higher wettability) in comparison to H-terminated patterns (having lower wettability).
	Pulsed DC magnetron sputtering	nc-carbon [present work]	Proliferation	> 500 %	3 days	•Enhancement in surface energy increases the cell-viability.
L-929	Plasma assisted CVD	carbon-nanowalls layers [30]	Adhesivity			•Superhydrophobic surfaces have an inhibitory effect for cell-growth.
	Pyrolysis	Micro-patterned carbon [31]	Cytotoxicity	negative effect	3 days, 5 days	•The reduction was lower in patterned carbon surface in comparison to smooth surface.
	Impregnation	Carbon-carbon composite [32]	Proliferation	No effect		•No effect on cell-viability at 4 μm^3/cell and lower concentrations. •Composites at 40 μm^3/cell showed cytotoxicity.
	Electro-spinning	Carbon nano-fibers/a-C films [33]		No effect	6 days	•The number of metabolically active cells on carbon fibrous structures were marginally more than control/films.
	RF magnetron sputtering	Diamond like carbon [34]		~ 20 %	1 day	• after 3 days increase in below than 5 %. • higher wetting (by N doping) better proliferation
	DC Sputtering	Conductive carbon [18]		~100 %	5 days	• Higher conductivity increases the cell growth.
	Pulsed DC magnetron sputtering	nc-carbon [present work]		> 200 %	5 days	•Enhancement in sp^2 content increases the cell-viability.

correlated to the enhancement of plasma density, whereas the role of pulse frequency can be correlated to two competing processes; neutralization of the ions and enhancement in ionization as well as kinetic energy of neutrals/ions. The stability of the films is ensured on the basis of surface energy results, where the huge variation in plasma power and pulsed frequency does not induce much

variation in surface energy values. Further, densification on increasing the pulse frequency supports the slight increase in crystallite size of graphite phase (sp^2 phase) as well as in the observed conversion of some sp^2 into sp^3 hybridization. Such finding is in agreement to the earlier reported works on carbon films [10,11]. The main role of plasma power enhancement is the reduction of nanodomain size. Such reduction increases the density of these nanodomains. Considering that the electrical conductivities of such nanodomains are reported higher at the periphery in comparison to the domain itself [17], such local variation of charge can induce local electric dipoles. The enhancement in such local dipoles density may be the prime factor for the observed excellent affinity of L-929 and Saos-2 cells in these films. However, it should be further emphasized that the key material property for governing the cell-viability can be different for different bio-cells. Overall, the present work provides a facile process to deposit nc-C films on low temperature, which can be used for cell-cultivation applications.

4. Conclusions

Low temperature carbon film fabrication is a processing challenge when one considers its use for large area deposition with high throughput. In present work, we have shown good quality carbon films with pulse DC plasma processing assisted with rotating substrate platform which restricts the substrate temperature well below 150 °C. The correlation of plasma parameters to the control of sp^3 and sp^2 hybridization has been established on the basis of detailed core level study of the films. The role of power density is found to control the plasma density, where as the role of pulse frequency is found to enhance the ionization and kinetic energies of ions/neutrals during the film deposition. These low-temperature processed carbon films show excellent cell-viability for the L-929 mouse fibroblast and Saos-2 bone cells.

Acknowledgements

This study was supported by the National Fusion Research Institute of Korea (NFRI) through the R&D Program of 'Plasma Advanced Technology for Agriculture and Food (Plasma Farming)' and the Global Development Research Center (GRDC), under the program of the Ministry of Science, ICT and Future Planning (MSIP, Grant No. 20120006672, 2nd stage 3rd year). Authors also acknowledge the help from Chikage Yamada and Seokyoung Yoon during the cell viability experiments.

References

[1] A.C. Ferrari, J. Robertson, Phil. Trans. R. Soc. Lond. A 362 (2004) 2477–2512.
[2] T. Sharda, S. Bhattacharyya, in: H.S. Nalwa (Ed.), Encyclopedia of Nanoscience and Nanotechnology vol. 2, American Scientific Publishers, California, USA, 2003, pp. 337–370.
[3] M.J. Burek, N.P. de Leon, B.J. Shields, B.J.M. Hausmann, Y. Chu, Q. Quan, A.S. Zibrov, H. Park, M.D. Lukin, M. Loncar, Nano Lett. 12 (2012) 6084–6089.
[4] D.H. Seo, S. Yick, D. Su, G. Wang, Z.J. Han, K. Ostrikov, Carbon 91 (2015) 386–394.
[5] U.A. Aregueta-Robles, A.J. Woolley, L.A. Poole-Warren, N.H. Lovell, R.A. Green, Front. Neuroeng. 7 (2014) 1–18.
[6] C. Portet, P.L. Taberna, P. Simon, E. Flahaut, C. Laberty-Robert, Electrochim. Acta 50 (2005) 4174–4181.
[7] H. Zhu, J. Wei, K. Wang, D. Wu, Sol. Energy Mater. Sol. C 93 (2009) 1461–1470.
[8] M. Bikshapathi, A. Sharma, A. Sharma, N. Verma, Chem. Eng. Res. Des. 89 (2011) 1737–1746.
[9] G.T. Teixidor, R.A. Gorkin, P.P. Tripathi, G.S. Bisht, M. Kulkarni, T.K. Maiti, T.K. Battacharyya, J.R. Subramaniam, A. Sharma, B.Y. Park, M. Madou, Biomed. Mater. 3 (2008) 034116.
[10] T.L. Parker, K.L. Parker, I.R. McColl, D.M. Grant, J.V. Wood, Diam. Rel. Mater. 3 (1994) 1120–1123.
[11] J. Miksovsky, A. Voss, R. Kozarova, T. Kocourek, P. Pisarik, G. Ceccone, W. Kulisch, M. Jelinek, M.D. Apostolova, J.P. Reithmaier, C. Popov, Appl. Surf. Sci. 297 (2014) 95–102.
[12] J.X. Piao, M. Kumar, A. Javid, S. Yoon, J.H. Lee, J.G. Han, Surf. Coat. Technol., communicated.
[13] P.K. Chu, L. Li, Mater. Chem. Phys. 96 (2006) 253–277.
[14] G.D. Yang, F. Liu, L. Wang, W.T. Wang, D. Wang, C.-S. Jiang, M.M. Al-Jassim, CrystEngComm 16 (2014) 10097–10102.
[15] H. Pedersen, C. Höglund, J. Birch, J. Jensen, A. Henry, Chem. Vap. Depos. 18 (2012) 221–224.
[16] X. Fan, K. Nose, D. Diao, T. Yoshida, Appl. Surf. Sci. 273 (2013) 816–823.
[17] A. Javid, M. Kumar, J.G. Han, RSC Adv. 5 (2015) 96360–96365.
[18] S.I. Kim, B.B. Sahu, S.E. Kim, A. Ali, E.H. Choi, J.G. Han, J. Mater. Chem. B 3 (2015) 3267–3278.
[19] S.I. Kim, B.B. Sahu, B.M. Weon, J.G. Han, J. Koskinen, S. Franssila, Jpn. J. Appl. Phys. 54 (2015) 010304.
[20] J.M. Yañez-Limón, F. Ruiz, J. González-Hernández, B.S. Chao, S.R. Ovshinsky, J. Appl. Phys. 78 (1995) 3015.
[21] J. Díaz, G. Paolicelli, S. Ferrer, F. Comin, Phys. Rev. B 54 (1996) 8064–8069.
[22] P. Mérel, M. Tabbal, M. Chaker, S. Moisa, J. Margot, Appl. Surf. Sci. 136 (1998) 105–110.
[23] L.G. Cançado, K. Takai, T. Enoki, M. Endo, Y.A. Kim, H. Mizusaki, A. Jorio, L.N. Coelho, R. Magalhães-Paniago, M.A. Pimenta, Appl. Phys. Lett. 88 (2006) 163106.
[24] A. Javid, M. Kumar, L. Wen, S. Yoon, S.B. Jin, J.H. Lee, J.G. Han, Mater. Des. 92 (2016) 405–413.
[25] A. Kozbial, Z. Li, C. Conaway, R. McGinley, S. Dhingra, V. Vahdat, F. Zhou, B. D'Urso, H. Liu, L. Li, Langmuir 30 (2014) 8598–8606.
[26] M. Allen, B. Myer, N. Rushton, J. Biomed. Mater. Res. 58 (2001) 319–328.
[27] M. Kalbacova, M. Kalbac, L. Dunsch, A. Kromka, M. Vaněček, B. Rezek, U. Hempel, S. Kmoch, Phys. Stat. Sol. B 244 (2007) 4356–4359.
[28] C. Popov, W. Kulisch, J.P. Reithmaier, T. Dostalova, M. Jelinek, N. Anspach, C. Hammann, Diam. Rel. Mater. 16 (2007) 735–739.
[29] B. Rezek, L. Michalikova, E. Ukraintsev, A. Kromka, M. Kalbacova, Sensors 9 (2009) 3549–3562.
[30] E.C. Stancu, M.D. Ionita, S. Vizireanu, A.M. Stancius, L. Moldovan, G. Dinescu, Mater. Sci. Eng. B 169 (2010) 119–122.
[31] M.M. Kulkarni, C.S. Sharma, A. Sharma, S. Kalmodia, B. Basu, J. Mater. Sci. 47 (2012) 3867–3875.
[32] G.I. Howling, E. Ingham, H. Sakoda, T.D. Stewart, J. Fisher, A. Antonarulrajah, S. Appleyard, B. Rand, J. Mater. Sci. Mater. Med. 15 (2004) 91–98.
[33] S. Jain, A. Sharma, B. Basu, J. Biomed. Mater. Res. B 101B (2013) 520–531.
[34] W.H. Liao, C.-R. Lin, D.-H. Wei, Y.-R. Shen, Y.-C. Li, J.-A. Lee, C.-Y. Liang, J. Biomed. Mater. Res. A 100A (2012) 3151–3156.